

XMM-Newton study of the Serpens star-forming region

T. Preibisch*

Max-Planck-Institut für Radioastronomie, Auf dem Hügel 69, 53121 Bonn, Germany

Received 23 June 2003 / Accepted 19 August 2003

Abstract. We analyze a *XMM-Newton* X-ray observation of the Serpens dark cloud with a total MOS-equivalent exposure time of 57 ksec. We find 45 individual X-ray sources. None of the class 0 protostars, only one of the class I protostars, and two of the flat-spectrum objects in the region are detected in X-rays. The optically invisible flat-spectrum source EC 95, a very young intermediate mass object, is the strongest X-ray source in the Serpens cloud. The analysis of its X-ray spectrum shows that the hydrogen column density towards EC 95 is considerably lower than expected from the extinction determined from near-IR spectroscopy and photometry. Possible reasons for this inconsistency are discussed.

Key words. open clusters and associations: individual: Serpens dark cloud – stars: formation – stars: coronae – stars: low-mass, brown dwarfs – stars: pre-main sequence – X-rays: stars

1. Introduction

The Serpens dark cloud is a nearby, very active star-forming region. The massive ($\sim 1500 M_{\odot}$) cloud core contains several mm sources that were identified as protostellar condensations (Testi & Sargent 1998), a number of far-infrared class 0 protostars (Hurt & Barsony 1996), at least 18 class I protostars (Kaas et al. 2000), and more than 150 near-infrared (NIR) sources (Strom et al. 1976; Eiroa & Casali 1992; Sogawa et al. 1997; Giovannetti et al. 1998; Kaas 1999). These objects constitute a dense and extremely young cluster. The Serpens cloud also displays further signposts of ongoing star-forming activity, such as Herbig Haro objects (Reipurth & Eiroa 1992), or molecular outflows (Eiroa et al. 1992; Huard et al. 1997; Herbst et al. 1997). As the extinction in the dark cloud reaches values up to ~ 50 mag (Sogawa et al. 1997), most of the young stellar objects (YSOs) are highly obscured, many are invisible at optical wavelengths. Recently, Lodieu et al. (2002) detected a young early L-type brown dwarf embedded in the Serpens cloud. The distance to the Serpens cloud is somewhat uncertain, with literature values ranging from 250 pc to 700 pc (see Eiroa 1991). De Lara et al. (1991) derived $d \sim 310$ pc from extinction measurements of several stars. Hogerheijde et al. (1999) argue that a distance of 400 pc might be more appropriate, but in order to be conservative we decided to use 310 pc for this work.

Young stellar objects in all evolutionary stages from class I protostars to ZAMS stars show highly elevated levels of X-ray activity. X-ray observations of star-forming regions allow to study the high energy processes in the YSOs (see review by Feigelson & Montmerle 1999). Since X-rays (with energies above ~ 1 keV) are much less affected by extinction than optical light, X-ray observations allow a deep look into dense

molecular cloud cores towards the embedded YSOs. In the last few years, X-ray emission could be detected from many deeply embedded infrared sources, mainly class I protostars, in several star-forming regions (e.g. Grosso et al. 1997; Feigelson & Montmerle 1999). These discoveries are of great importance for our understanding of the star formation process. For example, the X-ray emission from a YSO, which still is in its main accretion phase, should photoionize its circumstellar material and thus influence accretion as well as outflow processes, both of which are thought to be based on the interaction of ionized material with magnetic fields. The protostellar X-ray emission might even affect the formation of proto-planets in circumstellar disks (cf. Glassgold et al. 1997).

With its large number of embedded YSOs, the Serpens cloud is therefore a very interesting target for X-ray studies. The first X-ray observation of the Serpens cloud (Preibisch 1998) was performed with the ROSAT HRI and revealed seven individual X-ray sources within the $40' \times 40'$ field-of-view. One of the X-ray sources could be identified with the optically invisible infrared source EC 95, which is located in the central part of the cloud. An infrared spectroscopic follow-up study (Preibisch 1999) suggested this object to be a highly obscured ($A_V = 36$ mag), extremely young intermediate-mass ($\sim 4 M_{\odot}$) star. The strong extinction suggested an extraordinary high X-ray luminosity of $\sim 10^{33}$ erg s $^{-1}$ in the 0.1–2.4 keV ROSAT band. This luminosity estimate, however, was quite uncertain, because it was based on a very large extinction correction factor.

The *XMM-Newton* observatory has not only a much larger collecting area than ROSAT, but is also sensitive over a much wider energy band, extending from ~ 0.2 keV up to ~ 15 keV, what makes it much better suited to study the strongly extincted

* e-mail: preib@mpifr-bonn.mpg.de

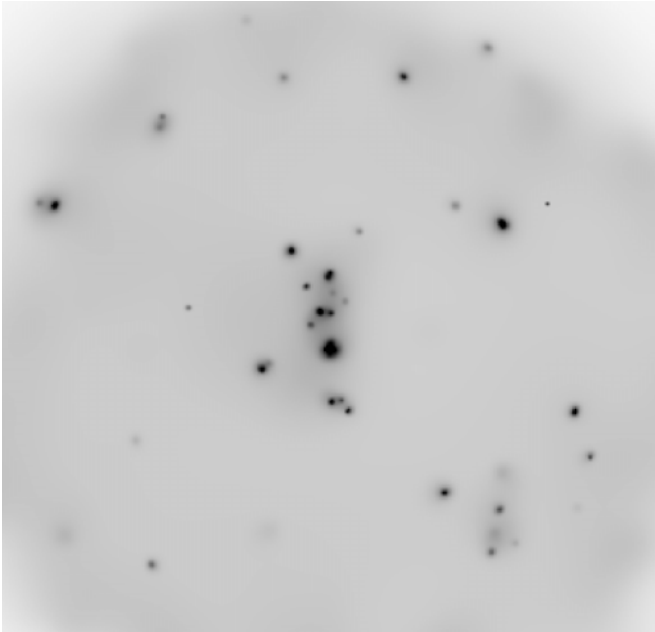


Fig. 1. The central $\sim 22' \times 22'$ region of the *XMM-Newton* image of the Serpens cloud. This image is the sum of the MOS1 + MOS2 + PN images, was smoothed with an adaptive filter (csmooth in CIAO) and is displayed with a square-root intensity scale. The bright central source is identified with EC 95.

and therefore very hard X-ray emission from highly obscured young objects.

2. Observations and data analysis

The observations discussed in this paper were obtained with the European Photon Imaging Cameras (EPIC) onboard *XMM-Newton*. The EPIC system (see Jansen et al. 2001) consists of two identical EPIC-MOS cameras (Turner et al. 2001) and the EPIC-PN camera (Strüder et al. 2001). The cameras were operated with the medium optical blocking filter and in the Full-Frame mode. They provide a $\approx 30'$ diameter field-of-view, energy coverage from ≈ 0.15 –15 keV, and moderate energy resolution ($E/\Delta E \approx 20$ –50). The *XMM-Newton* observation¹ of the Serpens cloud was obtained during the satellite revolution number 613 on 14 April 2003. The exposure times were 12.4 ksec for the MOS1 and the MOS2 camera, and 10.1 ksec for the PN camera. As the sensitivity of the PN camera is about 3 times higher than that of the individual MOS cameras for the case of the medium filter, the total MOS equivalent exposure time is about 57 ksec. Extraction of science products from the Observation Data Files followed standard procedures using the *XMM-Newton* Science Analysis System (SAS). We performed our data analysis with the most recent SAS version 5.4.1. We first investigated the total light curves of the cameras and found only small level variability, but no strong background flares during our observation. In our analysis of the individual X-ray

¹ We note that another observation with somewhat shorter exposure time was obtained two days earlier; these data, however, were strongly affected by a high, flaring radiation background and were therefore not used in our analysis.

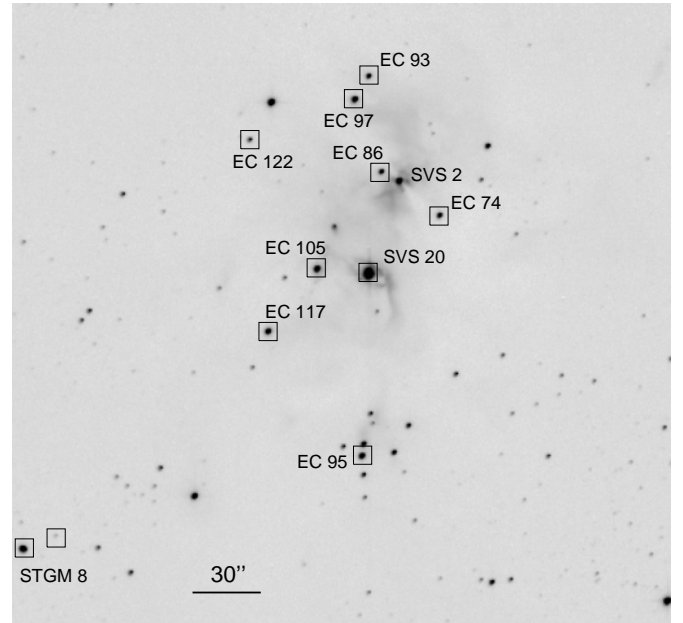


Fig. 2. Deep K-band image of the central part of the Serpens cloud, obtained by the author at the Calar Alto 3.5 m Telescope. The X-ray sources are marked by boxes and identified.

sources we concentrated on the data of the PN camera, which yields the highest signal (count rates).

2.1. Source detection and identification

Source detection was performed with the standard SAS detection pipeline on the summed (MOS1 + MOS2 + PN) dataset. A careful inspection of the X-ray images showed that the automatic detection retrieved all visually apparent X-ray sources correctly, but it also “detected” several spurious sources, which were then manually removed from the source list. This finally left us with 45 reliably detected X-ray sources, among them all 7 sources already detected by ROSAT (Preibisch 1998). We compared the source coordinates derived from the *XMM-Newton* data to optical (DSS) and near-infrared (2MASS) images and found no indications for systematic errors in the X-ray source positions. Table 1 provides a list of all X-ray sources in the field-of-view of our *XMM-Newton* observation. We denote these sources by names of the form XMMU JHHMMSS.S+DDMMSS based on their J2000 coordinates.

By inspection of the red DSS image we found reliable optical counterparts for 31 of the 45 X-ray sources. An inspection of the 2MASS K-band images revealed near-infrared counterparts for 11 of the 14 optically invisible X-ray sources. This leaves us with three X-ray sources for which we found neither an optical nor a near-infrared counterpart; all three sources are located in the outer parts of the X-ray image, more than $10'$ from the cluster center, and we suspect that they are (probably extragalactic) background objects, most likely active galactic nuclei.

Twelve of the X-ray sources, among them all the sources in the central part of the cloud, can be reliably identified with

Table 1. Properties of the X-ray sources in the Serpens cloud. The source names in the first column consist of the J2000 coordinates. The EPIC-PN countrates are listed in the second column, followed by information about optical and near-infrared counterparts and known membership to the Serpens cloud. The extinction and bolometric luminosity estimates in the next two columns were generally taken from Eiroa & Casali (1992), for 182957.9+011246 (=EC 95) they are based on the study by Preibisch (1999) and for 182957.7+011052 (=HD 170545) they were derived as described in the text. We then list the extinction-corrected X-ray luminosities in the [0.2–10] keV energy band and the fractional X-ray luminosities. The countrates for the two objects marked with asterisks have been derived from the MOS data and multiplied by the typical PN/MOS countrate ratio, because these sources are located outside the field-of-view of the PN image or in gaps between the individual chips.

Serpens J	CR_{PN} [cnts/s]	opt/NIR CP	$A_{\text{V,IR}}$ [mag]	L_{bol} [L_{\odot}]	L_{X} [erg/s]	$\log \frac{L_{\text{X}}}{L_{\text{bol}}}$	Identification
182904.5+010948	0.0247 ± 0.0043	y/y					
182920.5+010854	0.0265 ± 0.0035	y/y					
182922.8+011032	0.0433 ± 0.0039	y/y					
182926.5+011802	0.0139 ± 0.0025	-/-					
182931.3+010548	0.0118 ± 0.0025	y/y					
182933.1+011716	0.0676 ± 0.0043	y/y					SVS 14
182933.5+010700	0.0210 ± 0.0028	y/y					
182934.7+010528	0.0165 ± 0.0027	y/y					
182934.7+010606	0.0114 ± 0.0024	y/y					
182935.1+012338	$0.0318 \pm 0.0069^*$	-/y					
182939.7+011754	0.0080 ± 0.0017	-/y					
182941.5+010736	$0.0429 \pm 0.0057^*$	y/y					
182947.3+012234	0.0301 ± 0.0035	y/y					
182951.2+011640	0.0024 ± 0.0010	-/y M	16	0.90	$1.83\text{e}30$	-3.27	EC 53 = SMM5
182953.7+011702	0.0062 ± 0.0013	y/y M	2	0.41	$3.00\text{e}29$	-3.72	EC 67
182955.3+011034	0.0145 ± 0.0017	y/y					
182955.7+011428	0.0060 ± 0.0012	-/y M	13	1.13	$2.87\text{e}30$	-3.18	EC 74
182955.7+010024	0.0310 ± 0.0042	y/y					
182956.3+011056	0.0112 ± 0.0016	y/y					
182957.5+011448	0.0062 ± 0.0012	-/y M	2	0.32	$3.00\text{e}29$	-3.61	EC 86
182957.7+011052	0.0186 ± 0.0019	y/y ?	0.4	70	$6.38\text{e}29$	-5.62	HD 170545
182957.7+011404	0.0122 ± 0.0016	-/y M	19	57	$9.32\text{e}30$	-4.37	EC 90 = SVS 20
182957.9+011246	0.1466 ± 0.0044	-/y M	36	60	$3.70\text{e}31$	-3.79	EC 95
182957.9+011530	0.0159 ± 0.0021	-/y M	18	1.28	$1.21\text{e}31$	-2.61	EC 93
182958.4+011520	0.0119 ± 0.0019	y/y M	8	1.46	$2.88\text{e}30$	-3.29	EC 97
182959.3+011408	0.0231 ± 0.0020	y/y M	3	0.94	$1.62\text{e}30$	-3.35	EC 105
183000.7+011338	0.0097 ± 0.0014	-/y M	6	0.66	$1.58\text{e}30$	-3.21	EC 117
183001.3+011500	0.0090 ± 0.0014	-/y M					EC 122
183003.5+011620	0.0213 ± 0.0020	y/y M	0.5	0.48	$5.00\text{e}29$	-3.57	EC 135 = GGD 29
183004.7+012232	0.0111 ± 0.0024	-/-					
183006.3+010104	0.0135 ± 0.0031	y/y					
183006.4+010616	0.0065 ± 0.0016	y/y					
183006.7+011216	0.0055 ± 0.0014	-/y					
183007.7+011204	0.0282 ± 0.0025	y/y					STGM8
183008.1+010550	0.0050 ± 0.0016	y/y					
183010.0+012436	0.0113 ± 0.0029	-/-					
183018.3+011416	0.0112 ± 0.0017	y/y					
183022.0+012108	0.0134 ± 0.0027	y/y					
183022.4+012044	0.0163 ± 0.0028	y/y					
183023.5+010500	0.0192 ± 0.0029	y/y					
183025.9+010928	0.0078 ± 0.0017	y/y					
183035.5+010552	0.0108 ± 0.0027	y/y					
183037.5+011758	0.0742 ± 0.0054	y/y					
183039.8+011800	0.0192 ± 0.0032	y/y					
183040.2+011020	0.0068 ± 0.0022	y/y					

known cluster members from Eiroa & Casali (1992). The identifications are listed in Table 1.

2.2. Determination of countrates

With SAS we extracted the counts for all sources in circular apertures and in the [0.2–10] keV energy band. We generally used aperture radii of 15", which include 70% of the point-source flux. For some sources, smaller apertures had to be used due to the presence of other nearby sources; in these cases we used the appropriate PSF correction factor. We determined the exposure time for each source region and the background regions from the corresponding exposure maps. The mean source count rates were then computed by subtracting from the counts in the source regions the expected background counts, dividing by the exposure time, and applying the PSF correction factor. The resulting count rates are listed in Table 1. The brightest source in our data, EC 95, has a PN countrate of ~ 0.15 cts/s; therefore the “photon pile up” effect² is not a problem for our data.

2.3. Temporal variability

With SAS we extracted the lightcurves for all *XMM-Newton* sources and from several large, source-free, background regions. Visual inspection of the individual background-subtracted lightcurves revealed only small-amplitude count rate fluctuations (as expected from Poisson statistics), but none of the sources showed systematic or flare-like variability, which is frequently seen on other young stellar objects (e.g. Montmerle et al. 1983; Preibisch & Neuhäuser 1995; Feigelson et al. 2002a). This lack of flares is a consequence of the rather short exposure time of the observation and the rather small number of X-ray sources. Feigelson et al. (2002a) investigated the variability of solar-mass pre-main sequence stars in the Orion Nebula Cluster based on deep *Chandra* X-ray observations, and found that, on average, any T Tauri star in the ONC shows one flare every 1.4 days. If the same flare rate applies to the YSOs in Serpens, the probability for each of the 12 X-ray detected cluster members to show a flare during our 10.1 ksec observation is 8.3%. Elementary stochastic³ shows that the probability for observing no flare among the 12 source is 35.3%, nearly as high as the probability for observing one flare (38.4%). We conclude from this that the lack of observed flares is a statistical effect and not some peculiarity of the X-ray emitting YSOs in the Serpens cloud.

2.4. X-ray luminosities

A reliable determination of X-ray luminosities requires knowledge of the hydrogen column density (i.e. the extinction) and the temperature (distribution) of the emitting plasma. These

parameters can be derived from fits to the observed X-ray spectra, which, however, are only feasible for sources with at least some 100 counts. In our data, only the X-ray source J182957.9+011246, which is identified with the YSO EC 95, has enough (~ 1100) counts for spectral fitting, and a detailed analysis of its spectrum is described in detail in Sect. 4.1.

For the other X-ray sources we can only estimate X-ray luminosities by assuming a “typical” plasma temperature and using available information about the source extinction (mainly from the study by Eiroa & Casali 1992). We used the PIMMS⁴ tool to determine the transformation factor between count rate and (un-absorbed) X-ray flux and assumed a plasma temperature of $kT = 1$ keV (12 MK), a typical value for young X-ray sources (e.g. Feigelson & Montmerle 1999; Preibisch 1997; Preibisch & Zinnecker 2002). The resulting X-ray luminosities and L_X/L_{bol} ratios are listed in Table 1 and are in the typical range of values found for young stellar objects in other regions (e.g. Feigelson & Montmerle 1999; Preibisch & Zinnecker 2002). We have to stress that our X-ray luminosity estimates for the Serpens objects are subject to considerable uncertainty, since the plasma temperatures are unknown. Changing, for example, the assumed plasma temperature from $kT = 1$ keV to $kT = 3$ keV would decrease the luminosity estimates by factors of up to ~ 2 for objects with moderate extinction ($A_V \lesssim 10$ mag) and up to ~ 3 for objects with high extinction ($A_V \sim 20$ mag).

3. X-ray detections among the different object classes

Young stellar objects can be classified by their spectral index between the near-(2 μm) and mid-infrared (10 μm) into a (evolutionary) sequence from class 0 protostars to class III ZAMS stars, with “flat spectrum” objects in the transition between class I and class II (see Wilking et al. 2001).

3.1. Class 0 protostars

No matches of X-ray sources to one of the five known class 0 protostars in the Serpens cloud (Hurt & Barsony 1996) are found. This result agrees with the non-detection of class 0 protostars in other star-forming regions like for example NGC 1333 (Getman et al. 2002; Preibisch 2003). We note that Tsuboi et al. (2001) claimed the *Chandra* detection of two class 0 protostars in the Orion OMC-3 cloud, but the exact nature of these mm sources is not yet fully established.

3.2. Class I protostars

Among the 18 known class I protostars in the Serpens cloud (Kaas 1999), only one, EC 53, is clearly detected as an X-ray source. A careful inspection of the locations of the other class I protostars in our *XMM-Newton* images does not show any indication for the presence of an X-ray source in most cases.

² According to the *XMM-Newton* Users’ Handbook, photon pile up occurs only for PN count rates exceeding 8 cts/s.

³ Given the flare probability for each source of $p = 8.3\%$, the probability to observe k flares among the 12 sources is $P(k) = \binom{12}{k} p^k (1-p)^{12-k}$.

⁴ PIMMS is the Portable, Interactive Multi-Mission Simulator provided by the HEASARC Online Service; for further information see <http://heasarc.gsfc.nasa.gov/Tools/w3pimms.html>

At the locations of three class I protostars (EC 80, EC 88, and EC 102), the *XMM-Newton* images seem to indicate marginally enhanced numbers of X-ray counts, but due to the presence of very nearby sources, the detection of X-ray emission from these objects cannot be reliably established.

The low detection frequency of class I protostars in the Serpens cloud seems to be in contrast with other regions, for example the ρ Oph cloud, where 70% of all class I protostars were detected in a deep *Chandra* observation (Imanishi et al. 2002). One explanation is the rather poor sensitivity of our data, due to the quite short exposure time. Our detection limit for objects with an extinction of $A_V = 50\text{--}100$ mag and a plasma temperature of $kT = 3$ keV is $L_X \sim 1\text{--}2 \times 10^{30}$ erg s⁻¹, i.e. in the same order of magnitude as the typical luminosities of X-ray detected class I objects (cf. Imanishi et al. 2002). We note that our X-ray detected class I protostar, EC 53, has an extinction of only $A_V \sim 16$ mag, quite low for a class I object. The other class I protostars in the Serpens cloud may be just too deeply embedded to be detected in our data.

3.3. Flat spectrum objects

We detect X-ray emission from two of the flat-spectrum objects in the Serpens cloud, SVS 20 and EC 95. The optically invisible infrared source SVS 20 (=EC 90) is a 1.6'' binary (Eiroa et al. 1987; Huard et al. 1997), both components of which are flat spectrum objects (Haisch et al. 2002). The system is surrounded by an evacuated bipolar cavity, suggesting the presence of an outflow (Huard et al. 1997). SVS 20 is one of the most luminous sources in the Serpens cloud; its components seem to be relatively massive YSOs with $\sim 1\text{--}3 M_\odot$. The X-ray luminosity we derive for SVS 20 is quite high, but the fractional X-ray luminosity is the lowest among the known cluster members. We note that the fractional X-ray luminosity of $\log(L_X/L_{\text{bol}}) \sim -4.4$ is in the typical range for YSOs somewhat more massive than the Sun (e.g. Feigelson et al. 2002b).

The other X-ray detected flat spectrum object, EC 95, will be discussed in detail in Sect. 4.

3.4. Class II and III objects

Most of the X-ray sources in the dark cloud are class II or class III objects, i.e. T Tauri stars. Their X-ray luminosities are in the typical range for T Tauri stars in other regions, e.g. IC 348 (Preibisch & Zinnecker 2002) or NGC 1333 (Preibisch 2003). The only exception is the class II object EC 93, which has an exceptionally high X-ray luminosity; with $\log(L_X/L_{\text{bol}}) = -2.6$, it belongs to the most X-ray active T Tauri stars.

3.5. The A-type star HD 170545

One of our X-ray sources is identified with the optically bright star HD 170545. It is unclear whether this star is related to the Serpens dark cloud or not. HD 170545 is a A0 type star and forms a 6.7'' binary with the fainter star PPM 165957. Its color of $B - V = 0.15$ suggests an extinction of $A_V \sim 0.4$ mag. If

we assume this star to be on the main-sequence, its photometric parallax is ~ 290 pc, i.e. only very slightly less than the assumed distance to the Serpens cloud of ~ 310 pc. If HD 170545 were a background star, it should be strongly reddened, as it is projected onto dense parts of the dark cloud. As it is only very slightly reddened, it cannot be a background object and therefore is probably related to the Serpens star-forming region, situated on the near side of the cloud. Assuming HD 170545 to be a cluster member, we derive an X-ray luminosity of $L_X = 6.4 \times 10^{29}$ erg s⁻¹ and $\log(L_X/L_{\text{bol}}) = -5.6$.

This X-ray detection is interesting, because the intermediate-mass A-type stars are not expected to show intrinsic X-ray emission, since they lack both, the magnetically driven X-ray emitting coronae of low-mass stars, and the strong high-mass stellar winds in which internal shocks can cause X-ray emission (see discussion in Preibisch & Zinnecker 2001). The most likely explanation for the observed X-ray emission is that it originates not from the A star itself, but from an unresolved T Tauri star companion. This assumption is supported by the observed X-ray luminosity, which is in the typical range for T Tauri stars.

3.6. The Brown Dwarf BD-Ser 1

Recently, Lodieu et al. (2002) presented a spectroscopic and photometric study of an object in the Serpens cloud, and found it to be an early L-type brown dwarf with an estimated mass of about $0.05 M_\odot$. This object, called BD-Ser 1, is the first confirmed very young L-type brown dwarf; it is still embedded in the molecular cloud and therefore suffers a quite large extinction of $A_V \sim 11$ mag.

During the last few years, X-ray emission has been detected from a number of (mostly young) brown dwarfs (see e.g. Neuhauser & Comerón 1998; Neuhauser et al. 1999; Rutledge et al. 2000; Imanishi et al. 2001; Preibisch & Zinnecker 2001, 2002). The typical fractional X-ray luminosities of the young brown dwarfs are $\log(L_X/L_{\text{bol}}) \sim -4$ to -3 , i.e. similar to the values found for late-type stars. However, all X-ray detected brown dwarfs are late M-type objects, no X-ray emission from an L-dwarf has yet been detected. The reason for this may be that the young M-type substellar objects are still warm enough to maintain partially ionized atmospheres which are capable of sustaining electrical currents, while in the cooler neutral atmospheres of L and T dwarfs such currents are shut off, preventing the buildup of magnetic free energy and the support for magnetically heated chromospheres and coronae (see Fleming et al. 2000; Mohanty & Basri 2003).

Our *XMM-Newton* data show no X-ray source at the location of BD-Ser 1. As the object happens to lie just in one of the inter-chip gaps in our EPIC-PN image, we used the EPIC-MOS images to derive an upper limit to the count rate. We determined the number of counts in a source region centered on the infrared position of the brown dwarf and compared this number to the expected background counts estimated from a nearby source-free region. With the Bayesian statistics method described by Kraft et al. (1991) we derived a 95% confidence upper limit of <0.00025 cnts/s for the MOS countrate.

Assuming a plasma temperature of $kT = 1$ keV and an extinction of $A_V \sim 11$ mag, as determined by Lodieu et al. (2002), the upper limit to the X-ray luminosity is $L_X < 2.3 \times 10^{29}$ erg s⁻¹, implying a fractional X-ray luminosity of $\log(L_X/L_{\text{bol}}) < -2.4$. As the fractional X-ray luminosities of most X-ray detected brown dwarfs are significantly below this value, our upper limit is not particularly useful; our data are just not sensitive enough and the extinction of this object is too strong to probe it with our data for possible X-ray emission at levels typical for other X-ray detected brown dwarfs.

3.7. Jets and outflows

Since the *Chandra* detection of X-ray emission from HH 2 (Pravdo et al. 2001), it is clear that in some jet bow shocks the shock-heated material can actually produce observable soft X-ray emission at levels of a few times 10^{29} erg s⁻¹. Until now, HH 2 seems to be the only X-ray detected HH object; further detections would therefore strongly improve the understanding of the processes giving rise to the observed emission.

The Serpens star-forming region contains numerous outflows and Herbig-Haro (HH) objects (see e.g. Reipurth & Eiroa 1992; Davis et al. 1999). However, none of our X-ray sources can be identified with an HH object or other outflow tracer⁵. Inspection of our *XMM-Newton* images at the locations of HH 106-107 and HH 455-460 revealed no indication for enhanced numbers of X-ray counts at any of these locations. This non-detection may be related to the rather poor sensitivity of our relatively short exposure *XMM-Newton* data. Also, the expected X-ray emission from shocks depends strongly on the shock velocity and density (cf. Raga et al. 2002), and the HH shocks in the Serpens cloud might perhaps just be too weak to produce detectable X-rays.

4. X-ray properties of EC 95

The optically invisible infrared source EC 95 is the brightest X-ray source⁶ in our *XMM-Newton* image. X-ray emission from this object was first discovered in a ROSAT observation (Preibisch 1998). Preibisch (1999) performed near-infrared spectroscopy for EC 95 and derived an spectral type K2, an extinction of $A_V \sim 36$ mag and a bolometric luminosity of

⁵ We note that we detect X-ray emission from the YSO EC 105, which seems to be associated with a molecular hydrogen outflow (Herbst et al. 1997). The characteristics of the observed X-ray emission, however, is fully consistent with the assumption of coronal emission from the young star EC 105, and there is no indication for any contribution from the outflow. Also, it is not clear whether the source of the outflow actually is EC 105 or a nearby deeply embedded object (SMM-3; see Herbst et al. 1997).

⁶ We note that the previous analysis of the ROSAT data could not fully exclude the possibility that the faint X-ray emission (~ 20 source counts) might come from EC 92, 5" to the north, rather than from EC 95. In our *XMM-Newton* image, this source has more than 1000 counts and we could achieve a much better astrometric calibration due to the larger number of detected sources. Our analysis clearly shows that the X-ray source is identified with EC 95, and not with EC 92.

$L_{\text{bol}} \sim 60 L_{\odot}$. While the near-infrared $J-H-K$ colors of EC 95 display only a very moderate infrared excess, recent $10 \mu\text{m}$ observations by Haisch et al. (2002) show a considerable mid-infrared excess; EC 95 can be classified as a ‘‘flat-spectrum’’ source, i.e. is a YSO in an evolutionary state between a very young class I protostar and a more evolved class II T Tauri star.

4.1. The *XMM-Newton* X-ray spectrum of EC 95

With SAS we extracted the pulse height spectrum for EC 95 from a circular source region and a suitable background spectrum from a nearby source-free region. We built the corresponding redistribution matrix files and ancillary response files appropriate for the position and size of the source extraction region and grouped the spectrum with 25 counts per bin. Spectral fitting was performed with the Sherpa package contained in the CIAO X-ray data analysis system (Freeman et al. 2002). We used the XSPEC model ‘‘raymond’’, describing the emission from a thermal plasma, and ‘‘wabs’’ for the absorption model. We fixed the abundances to a value of 0.3 times solar elemental abundances; this value is typical for young stellar objects (see e.g. Imanishi et al. 2002) and is also consistent with the strength of an Fe line in our spectrum (see below).

We started our spectral analysis with the most basic model, i.e. a single-temperature plasma plus absorption. This simple model yielded a statistically acceptable ($\chi^2 = 30.6$ for 43 degrees of freedom, $\chi^2/\nu = 0.71$) fit for the parameters $N_{\text{H}} = (3.37 \pm 0.13) \times 10^{22}$ cm⁻², $kT = (2.78 \pm 0.11)$ keV ($T = 32$ MK), and $EM = (2.83 \pm 0.11) \times 10^{54}$ cm⁻³. An extensive search of the parameter space with the MONTE-POWELL search-method confirmed these best-fit parameters. Figure 3 shows the observed spectrum together with the best-fit model. We also tried the ‘‘mekal’’ thermal plasma model instead of the ‘‘raymond’’ model; this yielded an equally good fit with almost identical fit parameters. We note that the spectrum shows a strong emission line at 6.7 keV, the K line of Fe XXIV and Fe XXV. The strength of this line directly confirms the 0.3 times solar abundances (at least for Fe) assumed in our fits. The spectral fit was also used to compute the intrinsic (extinction-corrected) X-ray luminosity by integrating the model source flux over the [0.2–10] keV band. The resulting value is $L_X = (3.7 \pm 0.2) \times 10^{31}$ erg s⁻¹, the fractional X-ray luminosity of EC 95 is therefore $\log(L_X/L_{\text{bol}}) = -3.8$.

While the fit with the single-temperature model is generally good, we note that the observed spectrum shows an excess of flux in the 1.8–2.0 keV range. Our attempts to reproduce this excess by varying individual element abundances (using the XSPEC model ‘‘vmekal’’) failed. We also note that a single-temperature model is only a crude approximation and cannot be fully correct, because it is well known that the coronae of active stars are generally *not* monothermal (e.g. Brickhouse et al. 2000; Sanz-Forcada et al. 2001). We therefore also fitted the spectrum with a two-temperature plasma model plus absorption and found the best-fit model ($\chi^2 = 28.1$ for 41 degrees of freedom, $\chi^2/\nu = 0.68$) for the following parameters: $N_{\text{H}} = (3.99 \pm 0.13) \times 10^{22}$ cm⁻², $kT_1 = (0.71 \pm 0.07)$ keV ($T_1 = 8$ MK), $EM_1 = (3.64 \pm 0.67) \times 10^{54}$ cm⁻³, $kT_2 = (3.00 \pm 0.14)$ keV

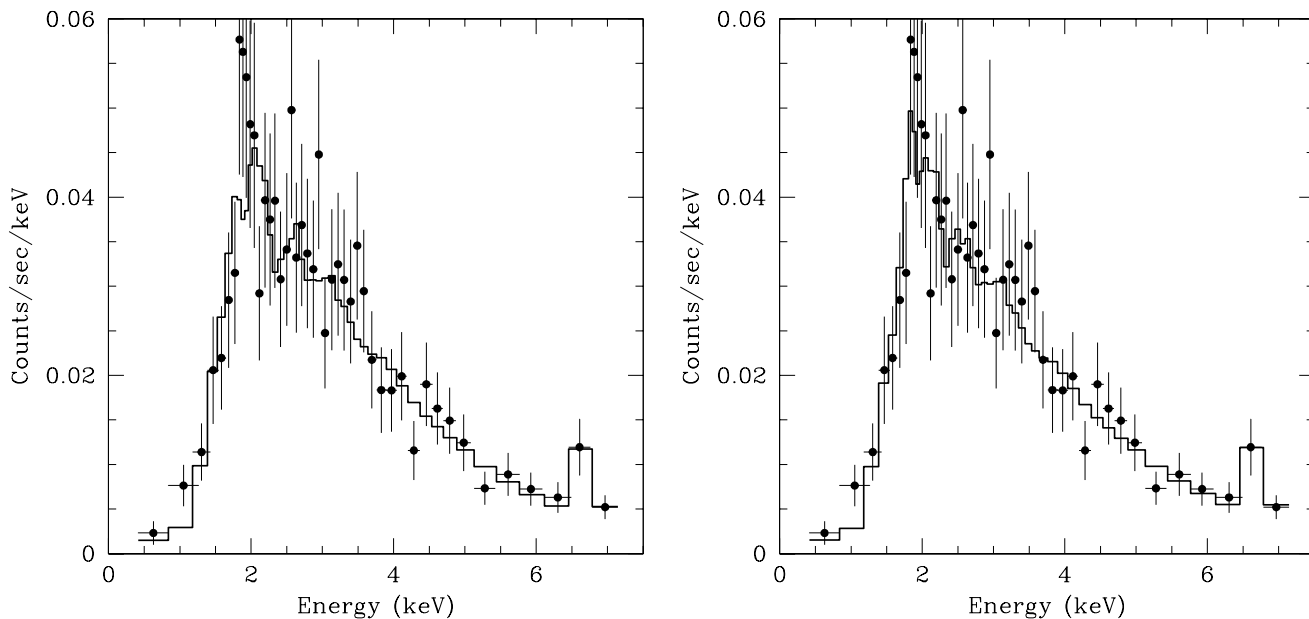


Fig. 3. The *XMM-Newton*-EPIC-PN spectrum of EC 95 (solid dots with error bars) together with the single-temperature fit (left) and the two-temperature fit (right) shown as histogram. Note the strong Fe emission line at 6.7 keV.

($T_2 = 35$ MK), and $EM_2 = (2.55 \pm 0.12) \times 10^{54} \text{ cm}^{-3}$. The intrinsic X-ray luminosity resulting from this fit is $L_X = (8.3 \pm 1.0) \times 10^{31} \text{ erg s}^{-1}$, the corresponding fractional X-ray luminosity is $\log(L_X/L_{\text{bol}}) = -3.44$.

The question now is: which of these two models provides a better description of the true spectrum? Whereas the two-temperature fit has a slightly higher statistical probability⁷ ($Q = 0.937$ as compared to $Q = 0.922$ for the one-temperature model) and fits the 1.8–2.0 keV part of the spectrum better, we note that the two-temperature model fitting parameters may indicate a potential problem: the low-temperature component produces significant flux only below $\lesssim 2$ keV, i.e. in that part of the spectrum, which is most strongly affected by the very high extinction. Although the emission measure of the low-temperature component is larger than that of the high-temperature component, it contributes only a very small amount of flux to the observed spectrum. This is exactly the kind of situation, for which spectral fitting simulations (see e.g. Maggio et al. 1995; Preibisch 1997) have shown that noise in the soft part of the spectrum might be easily mis-interpreted as a strongly absorbed low-temperature component, which actually does not exist. We therefore prefer the one-temperature fit. If the true temperature distribution in EC 95 would actually be better described by the two-temperature model, the plasma temperature and the X-ray luminosity derived from the one-temperature fit are still useful as lower limits.

The plasma temperature of ~ 32 MK is in the upper range typical for young stellar X-ray sources (e.g. Feigelson & Montmerle 1999; Preibisch 1997; Preibisch & Zinnecker 2002). The derived X-ray luminosity of $\sim 4 \times 10^{31} \text{ erg s}^{-1}$ places EC 95 on the top of the X-ray luminosity distribution of

young stellar objects (see e.g. Feigelson et al. 2002b; Preibisch & Zinnecker 2002), but is considerably smaller than the earlier estimate of $L_X \sim 10^{33} \text{ erg s}^{-1}$ based on the ROSAT data (Preibisch 1997). The reason for this difference lies in the fact that the ROSAT estimate was based on an assumed column density of $N_{\text{H}} \sim 7 \times 10^{22} \text{ cm}^{-2}$ as corresponding to the extinction derived from the near-infrared photometry and spectrum, $A_{V(\text{IR})} \sim 36$ mag. The *XMM-Newton* spectrum, however, yields a column density which is only about half as large and corresponds to a visual extinction of $A_{V(X)} \sim 17$ mag.

4.2. Clues to the extinction problem

Since both, the infrared extinction value and the X-ray spectral fitting result seem to be rather well constrained, this inconsistency is quite remarkable. Usually, the hydrogen column densities derived from the X-ray spectra of YSOs agree quite well to the optical or infrared extinction estimates. For example, Imanishi et al. (2001) compared the near-infrared colors of YSOs in the ρ Oph star-forming region with the hydrogen column densities from X-ray spectral fitting and found a good correlation. For some of their objects, mostly class I sources, the hydrogen column densities deduced from the X-ray spectra were much larger than expected from the near-infrared colors; they explain this effect by scattering of near-infrared light in the dense circumstellar material around these objects, what shifts the near-infrared colors towards more blue values. This, however, is exactly the opposite effect to what we find for EC 95, where the N_{H} value derived from the X-ray spectrum is considerably lower than the infrared extinction.

Very recently, Vuong et al. (2003) presented a determination of the gas-to-dust ratio in nearby dense clouds by comparing the total hydrogen column densities for class III sources, measured from their X-ray absorption, to the dust extinction

⁷ The statistical acceptance Q gives the probability that the deviations between the observed spectrum and the model spectrum are only due to statistical measurement errors (see e.g. Press et al. 1986).

in the near-infrared. For the ρ Oph star-forming region they found that the ratio $N_{\text{H,X}}/A_J$ is about 20% lower than the galactic standard value, what they explained as the consequence of differences in the metallicity of the local solar neighborhood ($d \lesssim 1$ kpc) and the general galactic metallicity. If this effect would also apply for EC 95, the discrepancy between the X-ray and infrared extinction would be somewhat smaller (a factor 1.7 rather than a factor 2), but still present and very significant. Metallicity effects are therefore not likely to be the solution of the extinction problem.

We note that similar discrepancies between X-ray and infrared extinction estimates were found for at least two other highly obscured YSO: SVS 16 in the NGC 1333 star-forming region (Preibisch 2003) and the protostellar binary system L1551 IRS 5 (Bally et al. 2003). Several models for the origin of the X-ray emission and the discrepancy of the X-ray and infrared extinction estimates in these objects have been discussed in Bally et al. (2003) and Preibisch (2003). Here we briefly summarize some possibilities and discuss whether they might apply for EC 95.

One possibility is X-ray emission from colliding stellar winds or outflows in a close binary system. As most of the stars in our galaxy are in multiple systems, EC 95 might well be a (yet unresolved) binary. Colliding stellar winds are capable to produce strong X-ray emission in tight O-star binary systems (e.g. Zhekov & Skinner 2000), and this scenario would offer an elegant solution of the “extinction problem”, because the stellar light could be strongly obscured by circumstellar material, whereas the X-rays emitted in the wind or outflow collision zone between the two stars would only suffer from the much lower extinction in the circumbinary and intra-cloud material. However, this model would have considerable problems to explain the very high X-ray luminosity of EC 95 and in particular the high plasma temperature⁸, these properties clearly require that at least the bulk of the X-ray emission is caused by some kind of magnetic activity.

Another possibility is that the X-ray emission from the stellar corona is not seen directly, but scattered into the line-of-sight by outer, circumstellar material. One might imagine favorable geometries (see Bally et al. 2003) in which the scattered X-rays would then suffer much less extinction than the direct light from the star that is strongly obscured by circumstellar disks seen nearly edge on. In this scenario, the intrinsic X-ray luminosity of the YSO should be much larger than the observed X-ray luminosity, because only a (presumably quite small) fraction of the X-rays is scattered in our direction. This is not a problem in the case of L1551 IRS 5 with its quite low observed X-ray luminosity; for EC 95, however, this would imply an extremely high intrinsic X-ray luminosity, considerably higher than that of all known coronal X-ray sources. We conclude that this scenario does not provide a satisfactory explanation.

The last possibility we discuss here was considered by Preibisch (2003) for the YSO SVS 16: the X-ray emitting

⁸ The observed plasma temperature of ~ 30 MK would require wind velocities of the order of ≥ 1000 km s⁻¹, much larger than typical for low-luminosity YSOs.

plasma might be displaced from the stellar surface and therefore could suffer much less extinction than the direct light from the star, that might be occulted by an edge-on disk. Applying the corresponding arguments to EC 95, we find that even under the extreme assumption that all X-ray emitting plasma is trapped in a single, huge coronal loop, this structure could hardly extend further out than about $9\times$ the stellar radius. Similar as in the case of SVS 16, the possibility that an extremely flat circumstellar disk seen perfectly edge-on could occult the light from the star but not a coronal loop extending only a few stellar radii above the stellar surface, appears very unlikely.

We conclude that the extinction problem remains mysterious. We note that all three objects, for which such a discrepancy of infrared and X-ray extinction estimates has been found so far, i.e. EC 95, SVS 16⁹, and L1551 IRS5, are flat-spectrum or class I objects, and all three objects belong to the most luminous YSOs in their respective star-forming regions. We can only speculate that there may be some peculiarity in these luminous embedded YSOs.

4.3. Radio emission from EC 95

Rodriguez et al. (1980) detected EC 95 in VLA observations as an unresolved ($<0.3''$) and very strong radio source. Smith et al. (1999) analyzed several VLA observations of EC 95 and derived radio luminosities of $\sim 8 \times 10^{16}$ erg s⁻¹/Hz at 3.5 cm and $\sim 1 \times 10^{17}$ erg s⁻¹/Hz at 6 cm. The radio spectral index is suggestive of optically thin synchrotron emission. In coronally active stars, this radio emission is usually interpreted as gyro-synchrotron radiation from electrons gyrating in the magnetic loops at the surface of these stars (cf. Montmerle et al. 1993). In the plot of X-ray versus radio luminosity (Güdel & Benz 1993), the revised X-ray luminosity of $L_X \sim 4 \times 10^{31}$ erg s⁻¹ places EC 95 just among the population of coronally very active “radio-bright” YSOs (cf. Montmerle et al. 1993). This supports a coronal emission mechanism for EC 95.

5. Summary and conclusions

Our *XMM-Newton* observation of the Serpens dark cloud reveals 45 individual X-ray sources. Despite the high sensitivity of *XMM-Newton* for hard X-ray emission as expected from deeply embedded young stellar objects, none of the known class 0 and only one of the known class I protostars in the cloud is detected as an X-ray source. For the optically invisible “flat-spectrum” infrared source EC 95, the remarkable inconsistency of the hydrogen column density derived from the X-ray spectrum and the extinction determined from the infrared photometry and spectroscopy remains puzzling. Its X-ray luminosity is very high, but not as extreme as suspected earlier from ROSAT data.

Acknowledgements. This work is based on observations with *XMM-Newton*, an ESA Science Mission with instruments and contributions directly funded by ESA member states and the USA (NASA). This

⁹ SVS 16 was recently confirmed to be a flat-spectrum source by Rebull et al. (2003).

publication makes use of data products from the Two Micron All Sky Survey, which is a joint project of the University of Massachusetts and the Infrared Processing and Analysis Center, funded by the National Aeronautics and Space Administration and the National Science Foundation.

References

- Bally, J., Feigelson, E., & Reipurth, B. 2003, *ApJ*, 584, 834
- Brickhouse, N. S., Dupree, A. K., Edgar, R. J., et al. 2000, *ApJ*, 530, 387
- Davis, C. J., Matthews, H. E., Ray, T. P., Dent, W. R. F., & Richer, J. S. 1999, *MNRAS*, 309, 141
- De Lara, E., Chavarría, K. C., & López-Molina, G. 1991, *A&A*, 243, 139
- Eiroa, C. 1991, in *Low Mass Star Formation in Southern Molecular Clouds*, ed. B. Reipurth, ESO Scientific Report, 11, 197
- Eiroa, C., & Casali, M. M. 1992, *A&A*, 262, 468
- Eiroa, C., Lenzen, R., Leinert, C., & Hodapp, K.-W. 1987, *A&A*, 179, 171
- Eiroa, C., Torrelles, J. M., Gomez, J. Fa, et al. 1992, *PASJ*, 44, 155
- Feigelson, E. D., & Montmerle, T. 1999, *ARA&A*, 37, 363
- Feigelson, E. D., Garmire, G. P., & Pravdo, S. H. 2002a, *ApJ*, 572, 335
- Feigelson, E. D., Bross, P., Gaffney III, J. A., et al. 2002b, *ApJ*, 574, 258
- Fleming, T. A., Giampapa, M. S., & Schmitt, J. H. M. M. 2000, *ApJ*, 533, 372
- Freeman, P. E., Kashyap, V., Rosner, R., & Lamb, D. Q. 2002, *ApJS*, 138, 185
- Getman, K. V., Feigelson, E. D., Townsley, L., et al. 2002, *ApJ*, 575, 354
- Gioannetti, P., Caux, E., Nadeau, D., & Monin, J.-L. 1998, *A&A*, 330, 990
- Glassgold, A. E., Najita, J., & Igea, J. 1997, *ApJ*, 480, 344
- Güdel, M., & Benz, A. O. 1993, *ApJ*, 405, L63
- Grosso, N., Montmerle, T., Feigelson, E. D., et al. 1997, *Nature*, 387, 56
- Haisch, K. E., Barsony, M., Greene, T. P., & Ressler, M. E. 2002, *AJ*, 124, 2841
- Herbst, T. M., Beckwith, S. V. W., & Robberto, M. 1997, *ApJ*, 486, L59
- Hogerheijde, M. R., van Dishoeck, E. F., Salverda, J. M., & Blake, G. A. 1999, *ApJ*, 513, 350
- Huard, T. L., Weintraub, D. A., & Kastner, J. H. 1997, *MNRAS*, 290, 598
- Hurt, R. L., & Barsony, M. 1996, *ApJ*, 460, L45
- Imanishi, K., Tsujimoto, M., & Koyama, K. 2002, *ApJ*, 572, 300
- Jansen, F., Lumb, D., Altieri, B., et al. 2001, *A&A*, 365, L1
- Kaas, A. A. 1999, *AJ*, 118, 558
- Kaas, A. A., Olofsson, G., & Bontemps, S. 2000, in *Star Formation from the small to the large scale*, 333rd ESLAB Symposium, ESA SP-445, 425
- Kraft, R. P., Burrows, D. N., & Nousek, J. A. 1991, *ApJ*, 374, 344
- Lodieu, N., Caux, E., Monin, J.-L., & Klotz, A. 2002, *A&A*, 383, L15
- Maggio, A., Sciortino, S., Collura, A., & Harnden Jr., F. R. 1995, *A&AS*, 10, 573
- Mohanty, S., & Basri, G. 2003, *ApJ*, 583, 451
- Montmerle, T., Koch-Miramond, L., Falgarone, E., & Grindlay, J. E. 1983, *ApJ*, 269, 182
- Montmerle, T., Feigelson, E. D., Bouvier, J., & André, P. 1993, in ed. E. H. Levy, & J. I. Lunine, *Protostars and planets III* (University of Arizona Press), 689
- Neuhäuser, R., & Comeron, F. 1998, *Science*, 282, 83
- Neuhäuser, R., Briceno, C., Comeron, et al. 1999, *A&A*, 343, 883
- Pravdo, S. H., Feigelson, E. D., Garmire, G., et al. 2001, *Nature*, 413, 708
- Preibisch, Th. 1997, *A&A*, 324, 690
- Preibisch, Th. 1998, *A&A*, 338, L25
- Preibisch, Th. 1999, *A&A*, 345, 583
- Preibisch, Th., & Zinnecker, H. 2001, *AJ*, 122, 866
- Preibisch, Th., & Zinnecker, H. 2002, *AJ*, 123, 1613
- Preibisch, Th., Neuhäuser, R., & Stanke, Th. 1998, *A&A*, 338, 923
- Preibisch, Th., & Neuhäuser, R. 1995, in *Flares and Flashes*, IAU Coll. 151, ed. J. Greiner, H. Duerbeck, & R. E. Gershberg, 212
- Press, W. H., Flannery, B. P., Teukolsky, S. A., & Vetterling, W. T. 1986, *Numerical recipes* (Cambridge University Press)
- Raga, A. C., Noriega-Crespo, A., & Velazquez, P. F. 2002, *ApJ*, 576, L149
- Rebull, L. M., Cole, D. M., Stapelfeldt, K. R., & Werner, M. W. 2003, *AJ*, 125, 2568
- Reipurth, B., & Eiroa, C. 1992, *A&A*, 256, L1
- Rodriguez, L. F., Moran, J. M., Ho, P. T. P., & Gottlieb, E. W. 1980, *ApJ*, 235, 845
- Rutledge, R. E., Basri, G., Martin, E. L., & Bildsten, L. 2000, *ApJ*, 538, L141
- Sanz-Forcada, J., Brickhouse, N. S., & Dupree, A. K. 2001, *ApJ*, 554, 1079
- Smith, K., Güdel, M., & Benz, A. O. 1999, *A&A*, 349, 475
- Sogawa, H., Tamura, M., Gately, I., & Merrill, K. M. 1997, *AJ*, 113, 1057
- Strom, S. E., Vrba, F., & Strom, K. M. 1976, *AJ*, 81, 314
- Strüder, L., Briel, U., Dennerl, K., et al. 2001, *A&A*, 365, L18
- Testi, L., & Sargent, A. I. 1998, *ApJ*, 508, L91
- Tsuboi, Y., Koyama, K., Hamaguchi, K., et al. 2001, *ApJ*, 554, 734
- Turner, M. J. L., Abbey, A., Arnaud, M., et al. 2001, *A&A*, 365, L27
- Vuong, M. H., Montmerle, T., Grosso, N., et al. 2003, *A&A*, in press
- Wilking, B., Bontemps, S., Schuler, R., Greene, T., & Andre, P. 2001, *ApJ*, 551, 357
- Zhekov, S. A., & Skinner, S. L. 2000, *ApJ*, 538, 808